Chinese Chemical Letters 32 (2021) 1367–1371

Contents lists available at ScienceDirect

Chinese Chemical Letters

journal homepage: www.elsevier.com/locate/cclet

Communication

A purely organic D-π-A-π-D emitter with thermally activated delayed fluorescence and room temperature phosphorescence for near-white OLED

Jing Sun[a,b], Junsen Jia[b], Bo Zhao[b], Jingjing Yang[b], Manjeet Singh[c], Zhongfu An[c,*], Hua Wang[b,*], Bingshe Xu[b], Wei Huang[a,*]

[a] Frontiers Science Center for Flexible Electronics, Xi'an Institute of Flexible Electronics (IFE) and Xi'an Institute of Biomedical Materials & Engineering, Northwestern Polytechnical University, Xi'an 710072, China
[b] Key Laboratory of Interface Science and Engineering in Advanced Materials, Taiyuan University of Technology, Ministry of Education, Taiyuan 030024, China
[c] Key Laboratory of Flexible Electronics (KLOFE) & Institute of Advanced Materials (IAM), Nanjing Tech University (NanjingTech), Nanjing 211816, China

ARTICLE INFO

Article history:
Received 5 August 2020
Received in revised form 22 September 2020
Accepted 30 September 2020
Available online 1 October 2020

Keywords:
Thermally activated delayed fluorescence
Room temperature phosphorescence
White OLED
D-π-A-π-D architecture

ABSTRACT

A purely organic D-π-A-π-D type emitter showing thermally activated delayed fluorescence (TADF) and room temperature phosphorescence (RTP) was designed and synthesized by utilizing the benzophenone as an acceptor and the *N*-phenyl-2-napthylamine as a donor moiety. It exhibits considerable TADF character in doped PMMA film and room temperature phosphorescence with a long lifetime of 74 ms at 466 nm in solid state. The devices with the configuration of ITO/Mo_2O_3 (4 nm)/mCP (30 nm)/mCP: x wt% NP2BP/TmTyPB (60 nm)/LiF (1.5 nm)/Al (100 nm) were prepared by vacuum evaporation to explore their electroluminescent performance. Interestingly, the non-doped device has obtained near-white emission with a fluorescence emission peak at 475 nm and a phosphorescence emission peak at 563 nm having the CIE coordinate of (0.23, 0.32) and the maximum external quantum efficiency of 1.09%.

Organic luminescent materials with the various donor (D) and acceptor (A) structure has attracted great attention owing to their potential application in organic light-emitting diodes (OLEDs) that can be the candidate for the next generation displays and advanced white lightings [1–4]. As known that, white organic light-emitting diodes (WOLEDs) reported so far are mainly prepared by utilizing the device structure of multiple emitting layers with double- or triple-color luminophores [5,6] or by doping multiple luminophores into the single emitting layer [7,8], leading to serious interface problems, phase separation and high cost of fabrication for high-quality WOLEDs. In contrast, single-molecular white light emitters can avoid such problems. It is worth mentioning that single molecular polymer incorporating double- or triple-colors functional groups showed excellent white light electroluminescent (EL) performance [9,10]. But the reproducibility of the polymer-based materials was not always satisfied for the devices because the repeatability and stability in the EL process cannot be ensured. In view of this, developing small single-molecular white light emitters with wide emission band covering the whole visible region would be an effective strategy to overcome the above mentioned problems. However, such materials were rarely reported suffering from the narrow emission band of small molecule light-emitting materials [11–13].

Recently, small single-molecular white light-emitting materials with D-A structure have been reported because of the existence of multiple excited states [14,15]. In 2017, Yan *et al.* put forwarded a class of *o*-carborane-based luminophores based on the donor (D)-acceptor (A) structure with strong charge transfer state which could realize multiple emission for double-color white light [16]. Meanwhile, Tang *et al.* reported a single organic molecule with dual phosphorescence at room temperature, which realized white light emission [17]. Moreover, Chi *et al.* also reported a small single molecule with white light emission consisting a blue fluorescent emission and yellow phosphorescent emission [18]. In 2018, Lee and coworkers designed and synthesized a thermally activated delayed fluorescence (TADF) emitter with dual conformations. One conformation showed the blue light emission and the other processed the orange light emission, which could be regulated and controlled by doping in host materials [19]. The device exhibited warm white light emission with a high maximum external quantum efficiency of 16.34%. In 2019, Yamamoto *et al.* identified

* Corresponding authors.
E-mail addresses: iamzfan@njtech.edu.cn (Z. An), wanghua001@tyut.edu.cn (H. Wang), iamwhuang@njtech.edu.cn (W. Huang).

https://doi.org/10.1016/j.cclet.2020.09.060
1001-8417/

carbazole-dibenzofuran dyads that showed two phosphorescence emission bands in the visible region. In the EL device, it exhibited good white light emission with a CIE coordinate of (0.319, 0.270) and a maximum external quantum yield of 0.6% [20]. On this basis, small single-molecular luminescent materials with multiple excited states could provide another radiative transition path to broaden the emission band for white light emission, especially in pure organic luminescent materials with room temperature phosphorescence (RTP) [21] and TADF character, which could simultaneously utilize the singlet and triplet excitons [22] to obtain the considerable luminous efficiency in the EL device. Moreover, these materials are heavy metal-free, which decreased the cost of materials and ensured the sustainable development. In addition, they exhibited good stability and processability performance to the benefit of high-quality luminescent devices.

Herein, we designed and synthesized a donor-π-acceptor-π-donor (D-π-A-π-D) type molecules in which benzophenone acts as acceptor and *N*-(2-naphthyl)aniline acts as donor (Fig. 1), which exhibited TADF character in doped PMMA film and RTPin solid state. More interestingly, in the EL device the phosphorescence emission can enhance that constitutes to the complementary color white light with external quantum efficiency (EQE) of 1.09%, indicating the potential application of RTP materials in the OLEDs.

The target compound was synthesized from 4,4′-dibromobenzophenone and *N*-(2-naphthyl)aniline by coupling reaction as shown in Scheme S1 (Supporting information) and fully characterized by ^{1}H NMR and ^{13}C NMR spectra (Figs. S1 and S2 in Supporting information). Thermal properties of NP2BP were characterized by thermogravimetric analysis (TGA) and differential scanning calorimetry (DSC) under nitrogen atmosphere (Fig. S3 in Supporting information). The decomposition temperature (T_d, corresponding to 5% weight loss) is 440 °C and the glass transition temperature (T_g) is 99 °C (Table 1), indicating its excellent thermal stability for high-quality OLEDs. The electrochemical properties of NP2BP were investigated by cyclic voltammetry (CV) (Fig. S4 in Supporting information). The highest occupied molecular orbital (HOMO) energy level (-5.508 eV) was calculated according to the oxidation potentials (1.010 V) against ferrocenium/ferrocene (F_{c+}/F_c). The lowest unoccupied molecular orbital (LUMO) energy level (-2.604 eV) was obtained from the equation of $E_{LUMO} = E_{HOMO} + E_g$ (the intersection of the absorption and emission spectra).

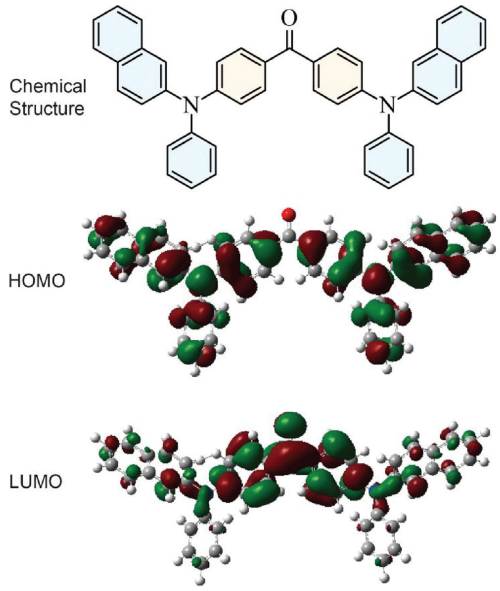

Fig. 1. The chemical structure and theoretical calculations of HOMO and LUMO distributions of NP2BP molecule.

The compound exhibited excellent solubility in different solvents. There existed a distinct absorption band at about 385 nm attributed to the charge transfer state from the donor *N*-(2-naphthyl)aniline to the acceptor benzophenone (Fig. 2a and Table 1). From PL spectra, we can see that NP2BP shows a solvatochromic effect [23,24] from low-polarity hexane (422 nm) to high-polarity acetonitrile (545 nm) (Fig. 2b). So, there is a large red-shift of 123 nm in fluorescence, and the full width at half maximum (FWHM) also increased with the increasing solvent polarity. Their Lippert-Mataga plot (Fig. 2c) shows a linear relationship, and the locally excited (LE) state and charge transfer (CT) state were well hybridized with the molecular dipole moments (μ_e) of 22.96 D [25]. From the density functional theory (DFT) calculations at the B3LYP/6-31 G(d) level based on Gaussian 03 package (Fig. 1), HOMO dispersed on *N*-(2-naphthyl) aniline groups and benzene ring of benzophenone, and LUMO was mainly distributed on benzophenone moieties, implying the effective CT state from the donor to the acceptor. On this basis, it convinces that this compound is a typical CT molecule and process stable composition and property upon the solvent polarizations [26]. Moreover, the lifetimes primarily prolonged and subsequently decreased with the increasing solvent polarity dominated by the transition from LE state to CT state (Fig. 2d). The photoluminescence and phosphorescence spectra in 2-MeTHF solution at low temperature were also measured (Fig. S5 in Supporting information). The triplet energy level was calculated to be 2.47 eV [27].

Owing to the large twisted configuration of the compound, we have investigated its TADF character (Figs. 3a–c). From the photoluminescence spectra at 77 and 298 K (Fig. 3a), we found that photoluminescence emission band had no obvious change, but phosphorescence emission band has a blue-shift with the increasing temperature closed to the photoluminescence emission band. It could be explained as that phosphorescence emission at 298 K was mainly from delayed fluorescence. According to the photoluminescence spectrum at 298 K and phosphorescence spectrum at 77 K, the singlet-triplet energy gap (ΔE_{ST}) was 0.19 eV, which could realize the reverse intersystem crossing (ISC) from T_1 to S_1 with the prolonged lifetime (Fig. 3b). However, the lifetime was in ms magnitudes longer than general TADF materials (μs magnitudes). It could be explained as that large ΔE_{ST} makes against the effective ISC process. Therefore, we investigated the photoluminescence spectra to verify the TADF character at different temperature (Fig. 3c and Fig. S6 in Supporting information). The photoluminescence emission peak enhanced with the increasing temperature from 100 K to 250 K, and then it decreased gradually when the temperature continued to increase. With the increasing temperature, the triplet excitons would be quenched [28]. Furthermore, photophysical properties of the compound in solid state were also recorded and depicted in Figs. 3d–f. At low temperature, there is a strong phosphorescence emission band (582 nm) with a weak phosphorescence emission (465 nm) observed after delaying 5 ms (Fig. 3d). At the room temperature, photoluminescence emission band at blue light region has no significant change but the intensity of phosphorescence emission band at 582 nm decreased due to the increasing temperature. Moreover, the delayed curves shown in Fig. 3e were measured at 466 nm and 570 nm. Both emission peaks exhibited the millisecond lifetimes of 73.93 ms (33.28%) and 17.42 ms (28.61%), respectively. It can be found that the lifetime at 466 nm was longer than that at 570 nm because triplet excitons at longer wavelength are more sensitive to the temperature. From the excitation-fluorescence mapping (Fig. 3f), we can see that there is no obvious change of emission peaks by increasing the excitation wavelength which is always located at 466 nm with a lifetime of

Table 1
The photophysical, thermal and electrochemical properties of NP2BP.

λ_{abs}[a] (nm)	λ_{PL} (nm)			τ (ms)		ΔE_{ST}[b] (eV)	Φ_c (%)	T_d/T_g (°C)	E_g (eV)	E_{HOMO}/E_{LUMO} (eV)
	Solution[a]	PMMA[b]	Solid	PMMA[c]	Solid[d]					
313, 381	488	477	466	143.79	73.93/17.42	0.19	16.3	440/99	2.90	−5.51/-2.60

[a] In 10^{-5} mol/L THF solution.
[b] PMMA film with 8 wt% doped concentration.
[c] Measured at 477 nm in PMMA film.
[d] Measured at 466 nm and 570 nm, respectively, in the solid state.

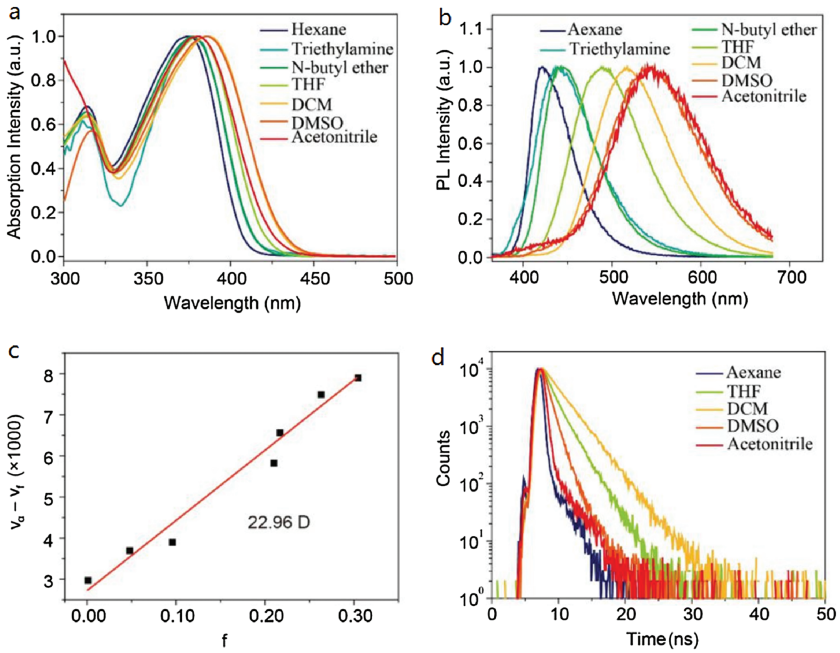

Fig. 2. Photophysical properties of NP2BP in different polar solvents. (a) UV–vis absorption spectra. (b) PL spectra. (c) Solvatochromic Lippert-Mataga models. (d) time-resolved decay curves of the emission band. a is in 10^{-5} mol/L solution; b and d are in 10^{-4} mol/L solution.

1.4 ns (Fig. S4). Meanwhile, it shows that the blue light (λ = 430 nm) can effectively excite the compound. However, total quantum yield (Φ_{total}) of the compound was only 16.3%. Furthermore, suffering from the large steric hindrance, the compound was difficult to cultivate the single crystal, therefore powder XRD were used to character the crystallization in the solid state. From the XRD pattern (Fig. S8 in Supporting information), it exhibited obviously sharp diffraction peaks (2θ) in the region of ($10^{\circ}\sim30^{\circ}$) indicating that considerable crystallization in the solid powder existed. The solid state provided a rigid environment to stabilize the triplet excitons and restrain the exciton quenching by molecular vibration and oxygen [29–31].

To evaluate the EL properties, non-doped and doped devices with the structure of ITO/Mo_2O_3 (4 nm)/mCP (30 nm)/mCP: x (x = 0, 5, 10 and 15) wt% NP2BP (30 nm)/TmTyPB (60 nm)/LiF (1.5 nm)/Al (100 nm) were prepared by evaporation process. In the non-doped devices (Fig. S9 in Supporting information), the compound acted as the single emitting layer. Interestingly, EL spectrum exhibited nearly white light emission consisting of double color with a blue emission at 475 nm and orange emission at 563 nm with a CIE coordinate of (0.23, 0.32) (Fig. 4a and Table 2). In the photoluminescence spectra, there is no exciplexes emission in the region from 500 nm to 600 nm excited by 365 nm UV lamp. Combined with the previous photophysical analysis, emission band at 563 nm in the EL process could be attributed to the phosphorescence signal that could effectively capture the triplet excitons to undergo radiative transitions from T_1 to S_0 [32–34]. Notably, maximum current efficiency, maximum power efficiency and external quantum efficiency (Figs. 4b and c) of the non-doped device were 2.29 cd/A, 1.37 lm/W and 1.09%, respectively. In order to investigate the EL properties, we also prepared the doped devices in which the compound was dispersed in the host materials of mCP maintaining the mono-molecular state. EL spectrum only shows blue emission at around 460 nm with a blue-shift compare with the non-doped devices because of the molecular aggregation. With increasing the doped concentration, blue emission shows a little red-shift due to the aggregation at the higher doping concentration (Fig. 4d) and it exhibited decent spectral stability at different driving voltages (Fig. S10 in Supporting information). Furthermore, the device with the concentration of 5% NP2BP possessed the best blue emission with the CIE coordinate of (0.15, 0.16) attributed to the local excited emission from the mono-molecular state in the doped devices [35]. However, its EL performance is not the best. In contrast, the device with the doped concentration of 15% NP2BP (Figs. 4e and f) exhibited the maximum current efficiency of 2.74 cd/A, the maximum power efficiency of 2.20 lm/W and external quantum efficiency of 1.69%, respectively. It could be attributed to the more effective utilization of triplet excitons in the high concentration which realize the delayed fluorescence by reverse ISC. Even though the doped film shows TADF character, its lifetime is too long because of large energy gap between S_1 and T_1 that leads to the low efficiency.

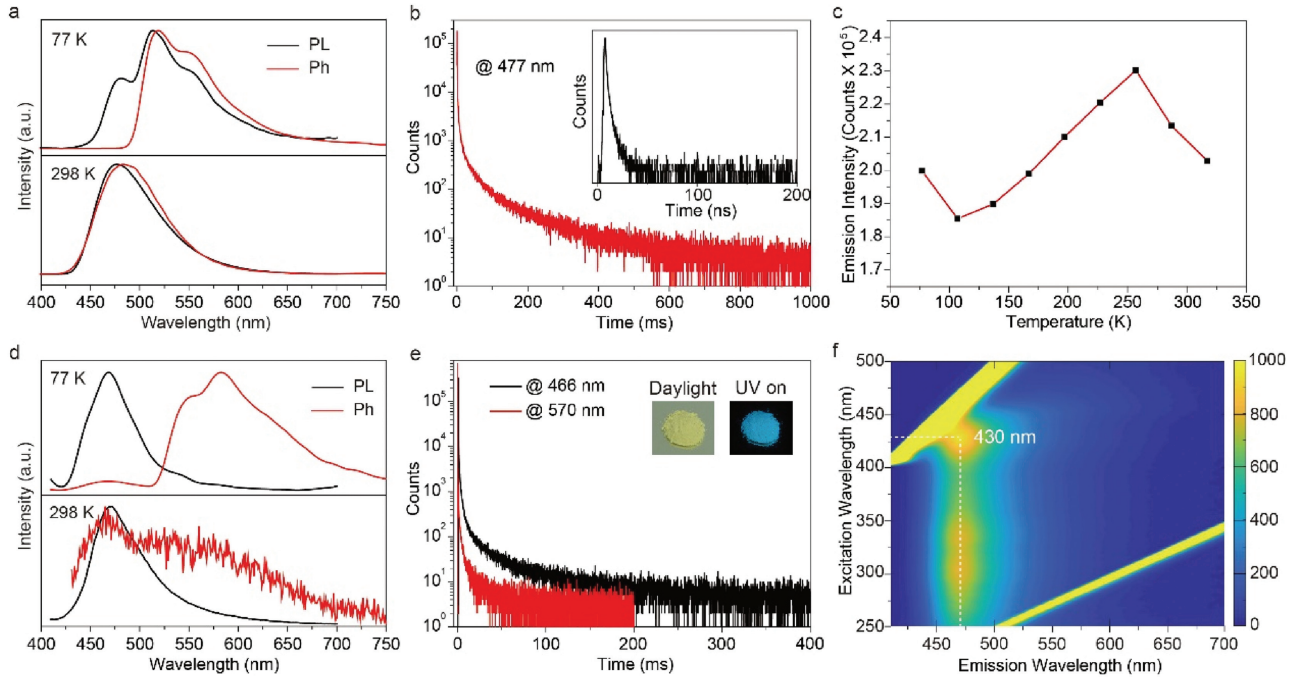

Fig. 3. Photophysical properties of NP2BP. (a) Photoluminescence and phosphorescence spectra of NP2BP doped in PMMA film at 77 K and 298 K. (b) Time-resolved decay curves measured at the emission band of 477 nm in PMMA film at room temperature. (c) The changes of luminescent intensity at variable temperature (From 77 K to 347 K) in doped PMMA film. (d) Photoluminescence and phosphorescence spectra of NP2BP solid measured at 77 K and 298 K. (e) Time-resolved decay curves measured in solid state at 466 nm and 570 nm at room temperature (Inset: Photographs under daylight and UV light). (f) The excitation-fluorescence mapping of solid at room temperature.

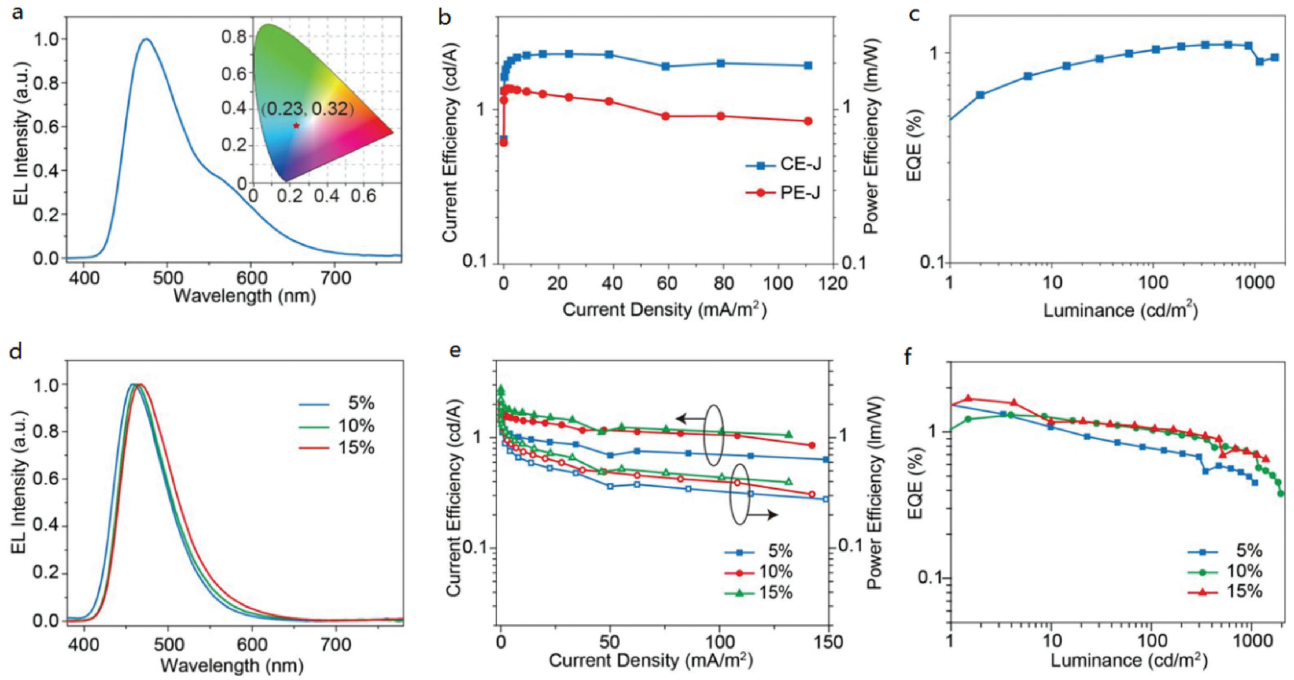

Fig. 4. EL performance. (a) EL spectra, the inset is CIE coordinates. (b) Current efficiency-luminance-power efficiency (CE-L-PE) curves. (c) The external quantum efficiency (EQE) curve of the non-doped devices. (d) EL spectra of devices with the concentration of 5%, 10% and 15%. (e) Current density-current efficiency-power efficiency (CE-J-PE) curves. (f) External quantum efficiency (EQE) curves (the concentration of 5%, 10% and 15%) of the doped devices.

In summary, we reported a donor-π-acceptor-π-donor (D-π-A-π-D) type blue fluorescent compound which exhibited excellent charge transfer characteristic in different polarity solvents. In particular, it possessed thermally activated delayed fluorescence (TADF) character in the doped PMMA film and considerable room temperature phosphorescence (RTP) in the solid state. Interestingly, the solid could be excited by the visible blue light (430 nm). Notably, the non-doped device using NP2BP as the single emitting layer exhibited the double-color near-white light emission with a CIE coordinate of (0.23, 0.32) and a maximum external quantum efficiency (EQE) of 1.09%. The doped devices (NP2BP:mCP = 5 wt%) also exhibited excellent blue light emission

Table 2
EL performance of non-doped and doped devices.

Devices	λ_{EL} (nm)	$V_{turn-on}$ (V)	L_{max} (cd/m^2)	CE_{max} (cd/A)	PE_{max} (lm/W)	EQE (%)	CIE
D0	475, 563	3.6	2395	2.29	1.37	1.09	(0.23, 0.32)
D5	457	3.6	1080	2.07	1.97	1.61	(0.15, 0.16)
D10	461	3.6	1994	1.90	1.55	1.30	(0.15, 0.17)
D15	465	3.9	1387	2.74	2.20	1.69	(0.16, 0.21)

with a CIE coordinate of (0.15, 0.16) and a maximum EQE of 1.61%. These results will provide guidance for their potential application in the OLEDs and further investigation based on pure organic compound with TADF and RTP characters is ongoing.

Declaration of competing interest

The authors declare that they have no known competing financial interests or personal relationships that could have appeared to influence the work reported in this paper.

Acknowledgments

This work had been absolutely supported by Program for National Natural Scientific Foundation of China (Nos. 91833304, 61904120, 61775155, 61705158); Natural Science Foundation of Shanxi Province (Nos. 201901D211090, 201903D121100, 201801D221124), the Fundamental Research Funds for the Central Universities, Shanxi Provincial Key Innovative Research Team in Science and Technology (No. 201601D021043), and the Joint Research Funds of Department of Science & Technology of Shaanxi Province and Northwestern Polytechnical University (No. 2020GXLH-Z-006).

Appendix A. Supplementary data

Supplementary material related to this article can be found, in the online version, at doi:https://doi.org/10.1016/j.cclet.2020.09.060.

References

[1] M.C. Gather, A. Köhnen, K. Meerholz, Adv Mater. 23 (2011) 233–248.
[2] P. Tao, S.J. Liu, W.Y. Wong, Adv. Opt. Mater. 8 (2020) 2000985.
[3] N. Sun, Q. Wang, Y. Zhao, et al., Adv Mater. 26 (2014) 1617–1621.
[4] B. Yang, J. Zhao, Z. Wang, et al., Chin. Chem. Lett. 30 (2019) 1969–1973.
[5] Y. Miao, K. Wang, L. Gao, et al., J. Mater. Chem. C 6 (2018) 8122–8134.
[6] P. Tao, W. Li, J. Zhang, et al., Adv. Funct. Mater. 26 (2016) 881–894.
[7] T. Higuchi, H. Nakanotani, C. Adachi, Adv Mater. 27 (2015) 2019–2023.
[8] Y. Li, H. Wu, C. Lam, et al., Org. Electron. 14 (2013) 1909–1915.
[9] Y. Wu, X. Li, H. Zhao, et al., Org. Electron. 76 (2020) 105487.
[10] J. Sun, D. Wu, L. Gao, et al., RSC Adv. 8 (2018) 1638–1646.
[11] K. Wang, Y. Shi, C. Zheng, et al., ACS Appl. Mater. Inter. 10 (2018) 31515–31525.
[12] J. Lee, H. Jung, H. Shin, et al., J. Mater. Chem. C 4 (2016) 2784–2792.
[13] C. Zhou, S. Zhang, Y. Gao, et al., Adv. Funct. Mater. 28 (2018) 1802407.
[14] V. Kumar, B. Sk, S. Kundu, A. Patra, J. Mater. Chem. C 6 (2018) 12086–12094.
[15] J. Guo, Z. Zhao, B. Tang, Adv. Optical Mater. 6 (2018) 1800264.
[16] D. Tu, P. Leong, S. Guo, et al., Angew. Chem. Int. Ed. 56 (2017) 11370–11374.
[17] Z. He, W. Zhao, J.W.Y. Lam, et al., Nat Commun. 8 (2017) 416.
[18] B. Xu, H. Wu, J. Chen, et al., Chem. Sci. 8 (3) (2017) 1909–1914.
[19] D. Li, F. Lu, J. Wang, et al., J. Am. Chem. Soc. 140 (2018) 1916–1923.
[20] K. Tabata, T. Yamada, H. Kita, Y. Yamamoto, Adv. Funct. Mater. 29 (2019) 1805824.
[21] X. Wang, N. Gan, M. Gu, et al., Chin. Chem. Lett. 30 (2019) 1935–1938.
[22] Y. He, N. Cheng, X. Xu, et al., Org. Electron. 64 (2019) 247–251.
[23] X. Tang, Q. Bai, Q. Peng, et al., Chem. Mater. 27 (2015) 7050–7057.
[24] S. Zhang, L. Yao, Q. Peng, et al., Adv. Funct. Mater. 25 (2015) 1755–1762.
[25] W. Li, Y. Pan, R. Xiao, et al., Adv. Funct. Mater. 24 (2014) 1609–1614.
[26] R.F. Jin, X.F. Zhang, W.M. Xiao, Molecules 25 (2020) 667.
[27] J. Sun, T. Zhang, X. Liao, et al., Tetrahedron 74 (2018) 1053–1058.
[28] K. Ling, H. Shi, H. Wang, et al., Adv. Optical Mater. (2019) 1901076.
[29] N. Gan, H. Shi, Z. An, W. Huang, Adv. Funct. Mater. 28 (2018) 1802657.
[30] J. Yang, X.M. Gao, Z.L. Xie, et al., Angew. Chem. Int. Ed. 56 (2017) 15299–15303.
[31] S. Cai, H. Ma, H. Shi, et al., Nat. Commun. 10 (2019) 4247.
[32] H. Han, Z. Tu, Z. Wu, Y. Zheng, Dyes Pigments 160 (2019) 863–871.
[33] J. Liu, P. Yuan, A. Liang, D. Ma, J. Lumin. 203 (2018) 83–89.
[34] F. Wang, J. Sun, M. Liu, et al., J. Mater. Chem. C 8 (2020) 1871–1878.
[35] T. Liu, L. Zhu, S. Gong, et al., Adv. Opt. Mater. 5 (2017) 1700145.